Climate Dynamics (2022) 58:961–979
https://doi.org/10.1007/s00382-021-05948-w

Asymmetric responses of the meridional ocean heat transport to climate warming and cooling in CESM

Qiuxian Li[1,2,3] · Yiyong Luo[1,2,3] · Fukai Liu[1,2,3]

Received: 5 June 2021 / Accepted: 21 August 2021 / Published online: 28 August 2021

Abstract
This study investigates the responses of the meridional ocean heat transport (OHT) to heat fluxes of equal amplitude but opposite sign into the global ocean surface using the Community Earth System Model (CESM). Results show that the poleward OHT in both hemispheres are weakened in response to the positive forcing (i.e., warming) and strengthened in response to the negative forcing (i.e., cooling), with the latter change exceeding the former, manifesting an overall asymmetric response. The OHT responses in the Indo-Pacific to both the warming and the cooling and thus their asymmetry are dominated by its Eulerian-mean component, due primarily to changes in the Indo-Pacific Subtropical Cells. Similarly, the OHT responses in the Atlantic are determined by changes in the Atlantic Meridional Overturning Circulation, yet their asymmetry is small due to the mediation from the nonlinear effect of temperature and velocity changes. For the Southern Ocean, the Eulerian-mean component still controls the total OHT responses, yet the largest contribution is from changes in vertical temperature structure. In addition, the asymmetric response in the Southern Ocean is a joint effort among the overturning circulation cells, horizontal gyres, eddies, as well as temperature changes.

Keywords Indo-Pacific Subtropical Cell · Atlantic Meridional Overturning Circulation · Meridional Ocean Heat Transport · Asymmetry

1 Introduction

The ocean plays a crucial role in maintaining the global energy balance and regulating the Earth's climate by transferring substantial amounts of heat from lower latitudes where the upper ocean absorbs heat from the atmosphere, to higher latitudes where the ocean releases heat into the atmosphere, leading to a poleward meridional ocean heat transport (OHT) in both hemispheres (Hsiung 1985; Trenberth and Solomon 1994; Macdonald and Wunsch 1996; Ganachaud and Wunsch 2000, 2003; Trenberth and Caron 2001; Ferrari and Ferreria 2011; Trenberth et al. 2019). The poleward OHT is a fundamental driving force of the climate system and has a crucial impact on the global climate (Hsiung 1985; Ganachaud and Wunsch 2000; Boccaletti et al. 2005). Therefore, it is important to understand the OHT as well as its response to climate change.

The processes that drive the OHT have been investigated in many previous studies. For example, Rahmstorf (2002) found that North Atlantic Deep Water (NADW) formation contributes largely to the OHT, while Simmons et al. (2004) suggested that the strength of abyssal mixing is crucial in maintaining the OHT. In addition, Held (2001) argued that wind-driven shallow circulations in the tropics and subtropics can effectively transport energy poleward, and this important role of wind forcing was verified in the study of Ferrari and Ferreria (2011). After a decomposition of the OHT into components from meridional overturning cell (i.e., the contribution from the time-mean overturning circulation in the meridional plane) and horizontal gyre (i.e., the heat transport by horizontal circulation), Bryan (1982) found

✉ Yiyong Luo
yiyongluo@ouc.edu.cn

✉ Fukai Liu
fliu@ouc.edu.cn

[1] Frontier Science Center for Deep Ocean Multispheres and Earth System (FDOMES) and Physical Oceanography Laboratory, Ocean University of China, Qingdao, China

[2] Laboratory for Ocean Dynamics and Climate, Qingdao Pilot National Laboratory for Marine Science and Technology, Qingdao, China

[3] College of Oceanic and Atmospheric Sciences, Ocean University of China, Qingdao, China

that the cell component dominates the OHT at low latitudes in both observations and models. Yang and Saenko (2012) also confirmed the dominate role of cell component at low latitudes, and they further found the OHT in the Southern Ocean and North Atlantic subpolar region are decided by the gyre component.

The OHT response to anthropogenic greenhouse gases (GHGs) has also been investigated as a hotspot, and it is generally recognized that the poleward OHT in both hemispheres is weakened under global warming (Yang and Saenko 2012; Yang et al. 2018; He et al. 2019; Donohoe et al. 2020). However, the mechanisms of this response are still under debate (Yang and Saenko 2012; Liu et al. 2018; He et al. 2019). Yang and Saenko (2012) examined the projected changes of the OHT in a warmer climate with the second generation Canadian Earth System Model (CanESM2). They found the weakened OHT in both hemispheres is largely determined by changes in the meridional cell, except in the subpolar Atlantic Ocean where the horizontal gyre circulation dominates. By using simulations from phase 5 of the Coupled Model Intercomparison Project (CMIP5) and version 4 of the Community Climate System Model (CCSM4), He et al. (2019) investigated the responses of the OHT and meridional atmosphere heat transport (AHT) to anthropogenic warming, and found that increased poleward AHT is compensated by a decrease in OHT in both hemispheres during the initial stage of warming, the latter is also determined by its cell component. Moreover, through decomposing the cell-induced heat transport into the advection of mean temperature by circulation anomaly ($\overline{T}V'$) and the advection of temperature anomaly by mean circulation ($\overline{V}T'$), they further showed that the cell heat transport change is generally dominated by the $\overline{T}V'$ related to the changes of the Indo-Pacific Subtropical cells (STC) and Atlantic Meridional Overturning Circulation (AMOC), except for the Southern Ocean where the $\overline{V}T'$ process dominates. The STC is mainly wind-driven (Mccreary and Lu 1994; McPhaden and Zhang 2002; Solomon and Zhang 2006; Farneti et al. 2014) and it slows down in response to a weakening of the subtropical winds under global warming (Luo et al. 2015; He et al. 2019). The AMOC is also projected to slow down due to the increased upper-ocean stratification in the North Atlantic subpolar region (Schmittner et al. 2005; Gregory et al. 2005; Weaver et al. 2007, 2012; Cheng et al. 2013; Jahn and Holland 2013; Rahmstorf et al. 2015; Zhu et al. 2015; Bakker et al. 2016; Liu et al. 2017a; Wen et al. 2018; Weijer et al. 2020). For the anomalous northward OHT in the Southern Ocean, in contrast to the finding by He et al. (2019), Liu et al. (2018) argued that it is resulted from the combined effect of increased stratification associated with CO_2 radiative forcing and Southern Ocean Meridional Overturning Circulation (SOMOC) change associated with strengthening and poleward shift of the westerlies. Addressing this controversy is one of our goals in the present study.

In addition to GHGs, anthropogenic aerosols (AAs) are another major external radiation forcing of climate change in the twentieth century. In general, GHGs acts to warm the climate while AAs cools the climate (Myhre et al. 2013). Both the emissions of GHGs and AAs experience a rapid increase over the last century (Myhre et al. 2013; Wang et al. 2016; Deng et al. 2020). However, while the OHT response to GHGs has been studied extensively, little attention has been paid to its response to AAs. Previous studies showed that regional oceanic responses to changes of AAs and GHGs forcings are overall opposite (Xie et al. 2013), but with the aerosol cooling effect exceeding the GHG warming effect. For example, Wang et al. (2016) found that the responses of the cross-equatorial gradient of sea surface temperature (SST) and sea level pressure (SLP) to AAs are greater in magnitude than those to GHGs. Li and Luo (2018) showed that the AAs-induced cooling in the southeastern tropical Indian Ocean is larger than the GHGs-induced warming. Through analyzing CMIP models, a recent study of Menary et al. (2020) found that the effects of AAs on AMOC evolution overwhelm those of GHGs, resulting in a strengthening of the AMOC from 1850 to 1985. However, it is not clear whether these asymmetries are a result of the magnitude difference of radiative forcing between GHGs and AAs or induced by their different spatial distributions. By analyzing 2000-yr heating and cooling experiments that are respectively forced by increased and decreased CO_2 concentration, Yang (2011) found that the equilibrium response timescale of ocean to opposite radiative forcings is asymmetric. The ocean response to decreased CO_2 can be twice as fast as to increased CO_2 because of the enhanced vertical mixing, convection, and overturning circulation after cooling. However, the radiative forcings applied to the climate system through perturbing CO_2 concentration are uncertain and may not be symmetric. To overcome the above difficulty, in this study we employ the NCAR's Community Earth System Model (CESM) to investigate the responses of the OHT to both climate warming and cooling by imposing "ghost" heat fluxes of equal amplitude but opposite sign into the ocean surface, so that the radiative forcing into the climate system is quantitative. Furthermore, since the warming and cooling forcings are perfectly symmetric, any asymmetry in OHT changes can be attributed to the intrinsically different oceanic responses to the forcings.

The rest of the paper is organized as follows. Section 2 describes the models, experiments, and metrics used in this study. Sections 3 and 4, respectively, present the responses of the MOC and OHT under the warming and cooling scenarios as well as their corresponding asymmetric changes, and discuss the formation mechanisms of these changes.

Finally, a summary and discussions of our findings are provided in Sect. 5.

2 Model experiments and analysis methods

2.1 CESM experiments

The CESM version 1.1 used here includes the Community Atmosphere Model version 5 (CAM5), the Community Land Model version 4 (CLM4) and the Parallel Ocean Program version 2 (POP2). The horizontal resolutions of atmosphere and land composition are 1.9° latitude × 2.5° longitude, with 30 atmospheric layers in the vertical. The horizontal resolution of the ocean composition is nominal 1°, telescoped meridionally to ~ 0.3° at the equator, with 60 uneven levels in the vertical.

Initializing from a long preindustrial simulation that is available at NCAR, we first integrate a control simulation (CTRL; Table 1) with no external forcing in the coupled atmosphere–ocean system. The warming and cooling simulations (HEAT and COOL) are then carried out through adding a uniform heat flux of 6 and -6 W m^{-2} into the ocean surface, respectively. The heat flux perturbation of 6 W m^{-2} in the study is chosen because this magnitude is comparable to the average forcing under abruptly quadrupled CO_2 ($4\times CO_2$) scenario (Gregory, 2004). Note the uniform heat flux Q^* of 6 or -6 W m^{-2} is added directly into the ocean component and modifies SST, which then influences the overlying atmosphere (sea ice) through air-sea (ice-sea) interaction. The total surface heat flux into the ocean Q_t can be expressed as:

$$Q_t = Q_{ao} + Q^*,$$

where Q_{ao} is the air-sea surface heat flux, which comprises the longwave radiation Q_{LW}, shortwave radiation Q_{SW}, latent heat flux Q_{LE}, and sensible heat flux Q_{SE}. These heat fluxes are computed interactively every time when the atmosphere and ocean communicate through the coupler. The responses to the warming and cooling forcings are defined as HEAT − CTRL and COOL − CTRL, respectively, and their sum [(HEAT − CTRL) + (COOL − CTRL)] is used to quantify their asymmetry. All the simulations are integrated for 250 years. Temporal evolution of the meridional overturning circulations and OHT in response to the warming and cooling forcings are shown Figs. 1 and 2, respectively. It can be seen that the AMOC, STC, and OHT reach an early quasi-equilibrium stage after 100 years of integration in both HEAT and COOL, and the responses appear to be

Table 1 Experiments with CESM1

Name	Run (years)	Description
CTRL	250	Control run
HEAT	250	Adding uniform 6 W m^{-2} to the ocean
COOL	250	Extracting uniform 6 W m^{-2} from the ocean

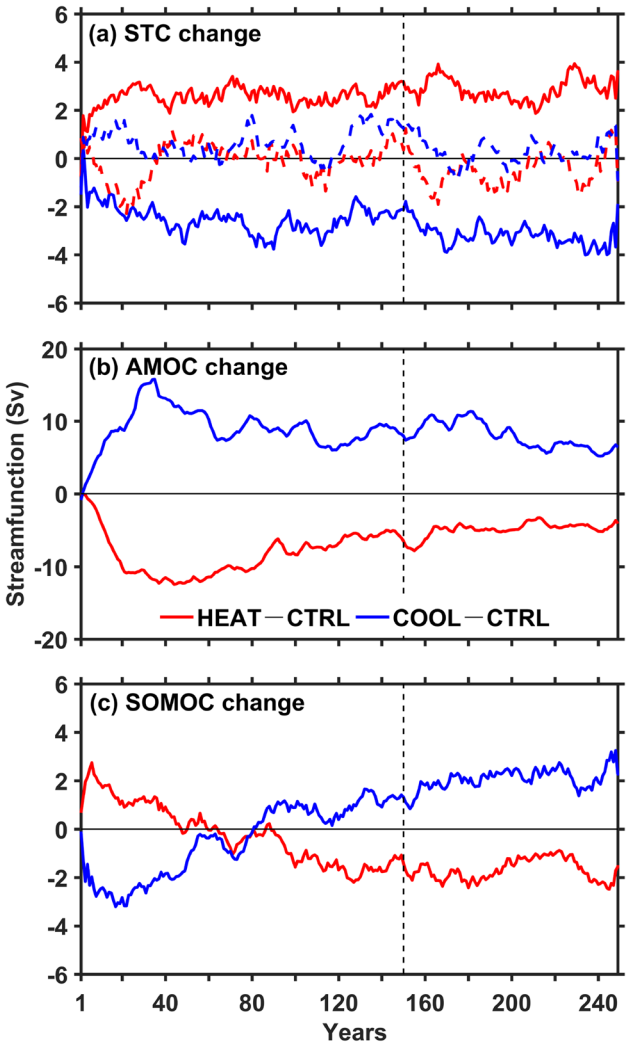

Fig. 1 Time series of changes in **a** STC (solid lines for its south hemisphere branch and dashed lines for its north hemisphere branch), **b** AMOC, and **c** SOMOC in response to the warming (red) and the cooling (blue). The northern (southern) hemisphere STC is defined as the maximum (minimum) streamfunction over 10°–30°N and 0–250 m (10°–30°S and 0–250 m); the AMOC strength is defined as the maximum streamfunction in 40°N; the SOMOC strength is defined as the maximum streamfunction at 49°S. The times series is smoothed with a 20-year running mean filter

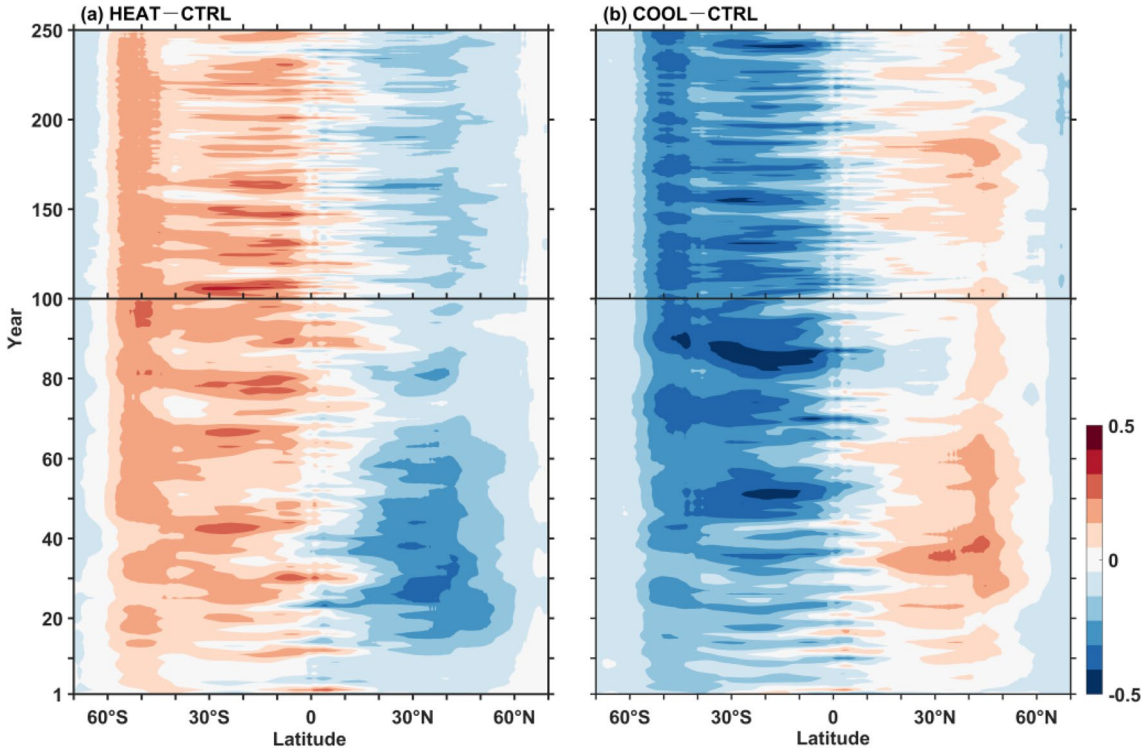

Fig. 2 Time-latitude diagram of the meridional ocean heat transport (OHT) change (PW; positive for northward transport): **a** HEAT-CTRL, and **b** COOL-CTRL. The times series in each latitude being smoothed with a 7-year running mean filter

asymmetric, with greater changes in COOL. Note that the SOMOC is still adjusting even after 150 years of integration (Fig. 1c). A mean of the model years 151–250 is taken for the following analysis. More details about the model and experiments can be found in Liu et al. (2017b).

2.2 CMIP6 simulations

To validate the simulated MOC response to the warming with CESM, we compare it to the solutions in the abruptly quadrupled CO_2 ($4\times CO_2$) and preindustrial control (piControl) simulations with CMIP6. The $4\times CO_2$ simulation represents an idealized global warming scenario, in which the concentration of carbon dioxide in the atmosphere instantly quadruples from its initial preindustrial value and then remains fixed. The CMIP6 climate models and their variables used in this study are shown in Table 2. The total MOC and the eddy-induced MOC are directly obtained from CMIP6 variables. The Eulerian-mean MOC is calculated as a difference between the total MOC and eddy-induced MOC. The MOC changes in CMIP6 models are defined as the difference between the averages over the last 100 years in the $4\times CO_2$ and the piControl runs. Only the first member run (r1i1p1) of each model is used to ensure equal weights in intermodel analysis.

Table 2 CMIP6 models and variables used in the analysis

Model	msftmz	msftmzmpa	msftmzsmpa
CESM2-WACCM-FV2	√	√	√
CESM2	√	√	√
CESM2-FV2	√	√	√
CESM2-WACCM	√	√	√
FGOALS-g3	√	√	–
MPI-ESM-1-2-HAM	√	√	–
MPI-ESM1-2-HR	√	√	–
MPI-ESM1-2-LR	√	√	–
CanESM5	√	√	–

'msftmz' is ocean meridional overturning mass streamfunction, denoting the total MOC; 'msftmzmpa' and 'msftmzsmpa' are ocean meridional overturning mass streamfunctions due to parameterized mesoscale and sub-mesoscale advections, respectively, with their sum denoteing the eddy-induced MOC. The Eulerian-mean MOC is calculated as a difference between the total MOC and eddy-induced MOC

2.3 Meridional overturning circulation

To quantify the MOC response, we calculate the meridional volume transport streamfunction by integrating meridional velocity (v) vertically from the bottom of the ocean to the surface, and then zonally from the western to the eastern boundaries. Furthermore, since the meridional

velocity (v) consists of Eulerian-mean velocity ($\overline{v}$) and eddy-induced velocity (v^*), the streamfunction can be decomposed into two components as below:

$$\psi_{Tot} = \iint_{-H}^{\theta} v dz dx = \iint_{-H}^{\theta} (\overline{v} + v^*) dz dx = \psi_{Eul} + \psi_{Ed}, \quad (1)$$

where x, y, and z are the zonal, meridional, and vertical coordinates, respectively. In CESM, the eddy-induced velocity is the sum of bolus velocity and sub-mesoscale velocity, both of which are obtained through parameterization (Gent and McWilliams 1990; Fox-Kemper et al. 2008). ψ_{Eul} and ψ_{Ed} represents the Eulerian-mean and eddy-induced MOC.

2.4 Meridional ocean heat transport

We integrate the temperature flux across an east–west section vertically and zonally to calculate the OHT (Bryan 1962, 1982; Hall and Bryden 1982):

$$\mathrm{OHT} = \rho_0 c_p \iint_{-H}^{\theta} v\theta dz dx, \quad (2)$$

where ρ_0 is seawater density, c_p is seawater specific heat, and θ is potential temperature.

In order to better understand the physical mechanisms involved in the OHT response to climate change, we decompose the OHT into contributions from Eulerian-mean flow, eddies and diffusion (Yang et al. 2015):

$$\begin{aligned} \mathrm{OHT_{Tot}} &= \rho_0 c_p \iint_{-H}^{\theta} \left(\overline{v}\theta + v^*\theta + D\right) dz dx \\ &= \mathrm{OHT_{Eul}} + \mathrm{OHT_{Ed}} + \mathrm{OHT_{Diff}}, \end{aligned} \quad (3)$$

where D denotes diffusion process.

In addition, the $\mathrm{OHT_{Eul}}$ is further decomposed into components associated with meridional overturning cells and horizontal gyres (Bryan 1982; Yang and Saenko 2012; He et al. 2019):

$$\begin{aligned} \mathrm{OHT_{Eul}} &= \rho_0 c_p \iint_{-H}^{\theta} \overline{v}\theta dz dx = \rho_0 c_p \iint_{-H}^{\theta} \left\{ [\overline{v}][\theta] + (\overline{v})(\theta) \right\} dz dx \\ &= \mathrm{OHT_{Cell}} + \mathrm{OHT_{Gyre}} \end{aligned} \quad (4)$$

where $[\cdot]$ represents the zonal average, and $(\cdot)$ represents the deviation from the zonal average. The $\mathrm{OHT_{Cell}}$ is the heat transport by the overturning cells (e.g., by the Indo-Pacific STC, the AMOC, and the SOMOC), while the $\mathrm{OHT_{Gyre}}$ is the heat transport by the horizontal gyres (e.g., by the subtropical gyre which is composed of warm poleward western boundary current and cold returning flow in the interior and eastern boundary).

Furthermore, to determine the contributions of anomalous velocity and temperature to the OHT anomaly, we decompose the $\mathrm{OHT_{Cell}}$ anomaly into three parts:

$$\begin{aligned} \Delta\mathrm{OHT_{Cell}} &= \rho_0 c_p \iint_{-H}^{\theta} \Delta\left([\overline{v}][\theta]\right) dz dx \\ &= \rho_0 c_p \iint_{-H}^{\theta} \left([\theta]\Delta[\overline{v}] + [\overline{v}]\Delta[\theta] + \Delta[\overline{v}]\Delta[\theta]\right) dz dx. \end{aligned} \quad (5)$$

Following Yu and Pritchard (2019), the three terms on the right-hand side of Eq. (5) are named as dynamic, thermodynamic, and nonlinear components, respectively. The dynamic component refers to the advection of mean temperature by circulation anomaly ($\overline{T}V'$), the thermodynamic component is the advection of temperature anomaly by mean circulation ($\overline{V}T'$), and the nonlinear component is calculated as a residual and represents the effect from correlation between temperature anomaly and velocity anomaly ($T'V'$).

3 Response of the MOC

Given the dominant role of the MOC in regulating the OHT, we first estimate the MOC and its responses to the warming and cooling. The MOC is presented in potential temperature-latitude coordinate. Specifically, the streamfunction is first calculated in depth-latitude coordinate, which is then projected to potential temperature-latitude coordinate by associating each depth with a mean potential temperature of that depth. Being evaluated in this way, the contribution of the MOC to heat transport can be estimated roughly by comparing the temperature difference between its upper and lower portions. For example, in the southern hemisphere subtropical region (contours in Fig. 3a), the counter-clockwise STC appears to contribute more to the OHT since it spans a larger temperature range (~ 16 ℃) than the clockwise AMOC (~ 9 ℃), and thus it plays a more important role for the poleward heat transport. Besides, the temperature-latitude coordinate can help to separate the warm wind-driven cells (mainly the STC) from the cold thermohaline cells (mostly the AMOC).

The climatological MOC and its response to the warming in CESM and CMIP6 are shown in Fig. 3 for comparison. Under the warming, the STC and AMOC slow down and the SOMOC shifts poleward (colors in Fig. 3a, b). While the Eulerian-mean component dominates the total MOC response over most regions (Fig. 3c, d), the eddy-induced component makes a contribution mainly in the Southern Ocean (south of 35°S) and works to offsets the Eulerian-mean counterpart (Fig. 3e, f). It can be seen that the results in CESM are overall consistent with those in CMIP6 simulations, suggesting that CESM does a reasonably good job in simulating the major patterns and responses of the MOC.

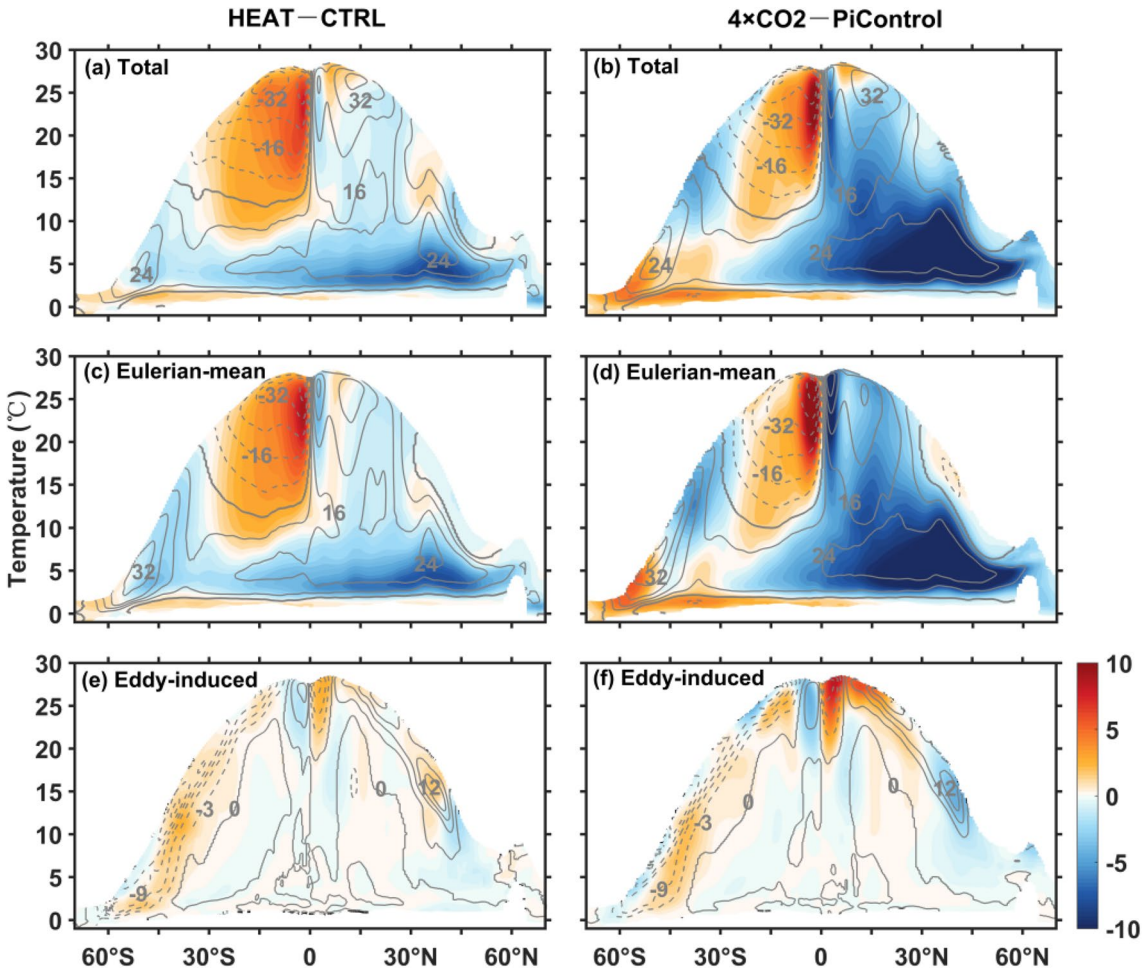

Fig. 3 The meridional overturning circulation (MOC) response (shading; Sv) to the warming in CESM (left) and CMIP6 (right). The MOC (**a**, **b**) is the residual of the Eulerian-mean component (**c**, **d**) and the eddy-induced component (**e**, **f**). The superimposed black contours are the MOC and its components in the corresponding control runs [solid lines for clockwise and dashed lines for anticlockwise; contour interval is 8 Sv in (**a**–**d**) and 3 Sv in (**e**–**f**)]. The nine CMIP6 models are CESM2-WACCM-FV2, FGOALS-g3, MPI-ESM-1-2-HAM, MPI-ESM1-2-HR, MPI-ESM1-2-LR, CanESM5, CESM2, CESM2-FV2, and CESM2-WACCM

Next, we will examine the MOC responses in each individual ocean basin to the warming and cooling as well as their asymmetry.

3.1 The Indo-Pacific STC

In the warmer climate, the Indo-Pacific STC is weakened in both hemispheres, but the weakening in the northern hemisphere is not as strong as that in the southern hemisphere (Fig. 4d). In the colder climate, on the contrary, the Indo-Pacific STC is strengthened in both hemispheres, also with a stronger response in the southern hemisphere (Fig. 4e). Their asymmetry largely resembles the cooling response in most regions except for the upper ocean between 20°S to the equator (Fig. 4f), indicating that the Indo-Pacific STC is more sensitive to the cooling than warming.

Since the STC is mainly wind-driven and its strength largely depends on the subtropical zonal winds (Mccreary and Lu 1994; McPhaden and Zhang 2002; Solomon and Zhang 2006; Farneti et al. 2014), we examine the changes in the zonal wind stress. The weakened (strengthened) Indo-Pacific STC (Fig. 4d, e) can indeed be explained by a reduction (an enhancement) of the easterlies roughly between 10° and 30° in both hemispheres (Fig. 5a). In the northern subtropics, the enhancement in response to the cooling exceeds the reduction in response to the warming, leading to a strengthening of the STC in their asymmetry (Fig. 4f). In the southern subtropics, however, the zonal wind response to the warming is greater (smaller) than that to the cooling north (south) of 18°S, resulting in a more complicated change of the STC there. The weakening (strengthening) of the subtropical winds under the warming (cooling) is closely related to the changes in the Hadley Cell (Fig. 6). Moreover, the asymmetry of the Hadley

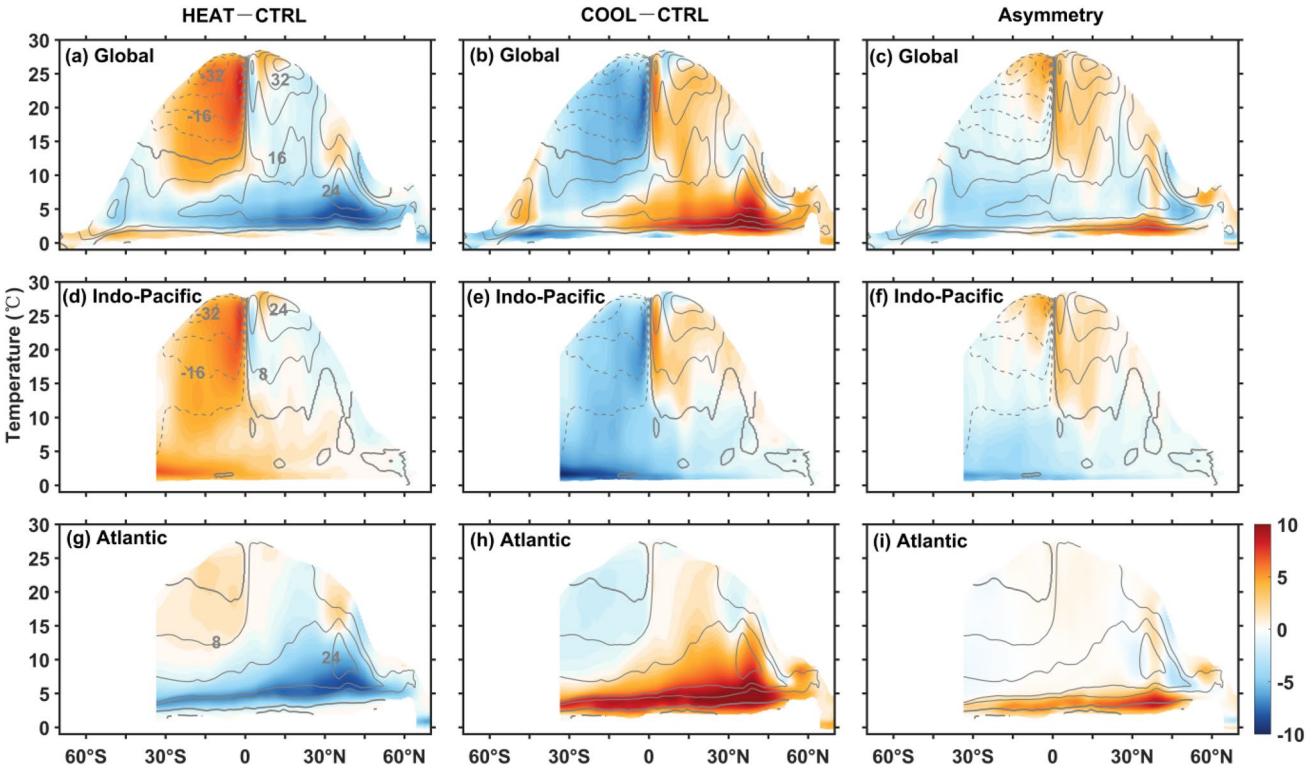

Fig. 4 The MOC Changes (shading; Sv) for the Global Ocean, the Indo-Pacific Ocean, and the Atlantic Ocean in response to the warming (left), the cooling (middle) and their corresponding asymmetry (right). The superimposed black contours are the MOC in CTRL (solid lines for clockwise and dashed lines for anticlockwise; contour interval is 8 Sv)

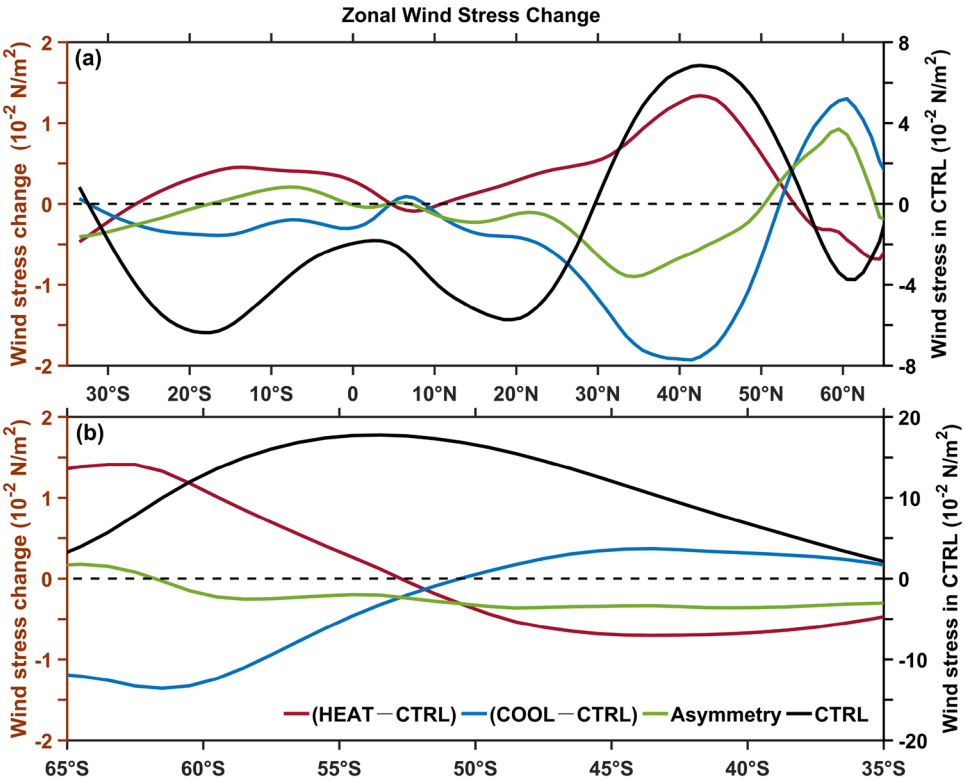

Fig. 5 Changes in zonal wind stress (right axis) over the Indo-Pacific Ocean (**a**) and the Southern Ocean (**b**) in response to the warming (red), the cooling (blue) and their corresponding asymmetry (green). The black line is the zonal wind stress in CTRL (left axis)

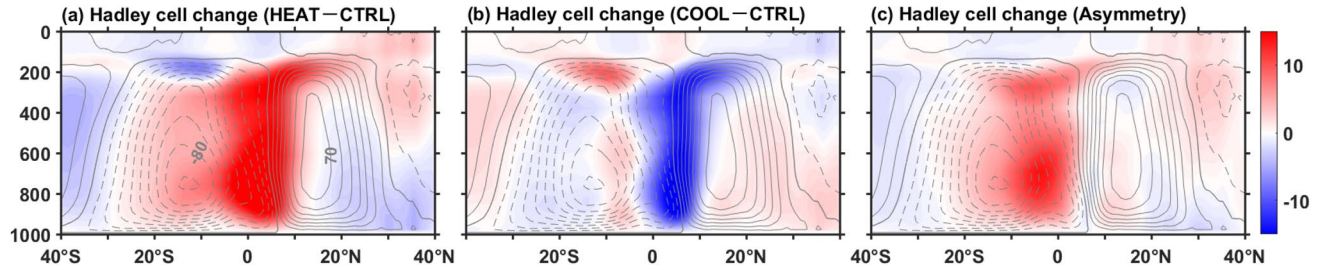

Fig. 6 Changes in the Hadley cell (shading; 10^9 kg s^{-1}) in response to the warming (**a**), the cooling (**b**) and their corresponding asymmetry (**c**). The superimposed black contours are the Hadley cell in CTRL (solid lines for clockwise and dashed lines for anticlockwise; contour interval is 10^{10} kg s^{-1})

Cell responses is consistent with that of the subtropical wind responses, and is responsible for the larger sensitivity of the wind stress in the southern subtropics. Another interesting feature in Fig. 6 is the intertropical convergence zone (ITCZ) shift induced by the warming or cooling. As the position of the ITCZ roughly coincides with the ascending branch of the Hadley Cell, the significant positive (negative) anomaly of streamfunction near the equator under the warming (cooling) represents a southward (northward) shift of the ITCZ (Fig. 6a, b). Following Adam et al. (2016), the ITCZ position (ϕ_{ITCZ}) is measured as the latitude of the maximum value of zonal mean precipitation (P) between $\phi_1 = 20°$S and $\phi_2 = 20°$N:

$$\phi_{ITCZ} = \frac{\int_{\phi_1}^{\phi_2} \phi[\cos(\phi)P]^{10} d\phi}{\int_{\phi_1}^{\phi_2} [\cos(\phi)P]^{10} d\phi}. \quad (6)$$

Result shows that the warming-induced northward shift of ~ 0.9° is smaller than the cooling-induced southward shift of ~ 1.6°. This asymmetry is likely due to that the stronger STC change under the cooling can alleviate the burden of meridional atmosphere heat transport to a larger extent (Green and Marshall 2017; Schneider 2017; Kang et al. 2018). Since this study focuses on the OHT response to different forcings, further investigation on the AHT response and ITCZ shift is left for future work.

3.2 The AMOC

The warming induces a weakening of the AMOC and a shoaling of its core (Fig. 4g), which is resulted mainly from a more buoyant surface ocean due to more heat and freshwater inputs into the ocean over the North Atlantic subpolar region (Fig. 7a, d). In contrast, under the cooling, the less buoyant subpolar surface ocean (Fig. 7b, e) enhances the

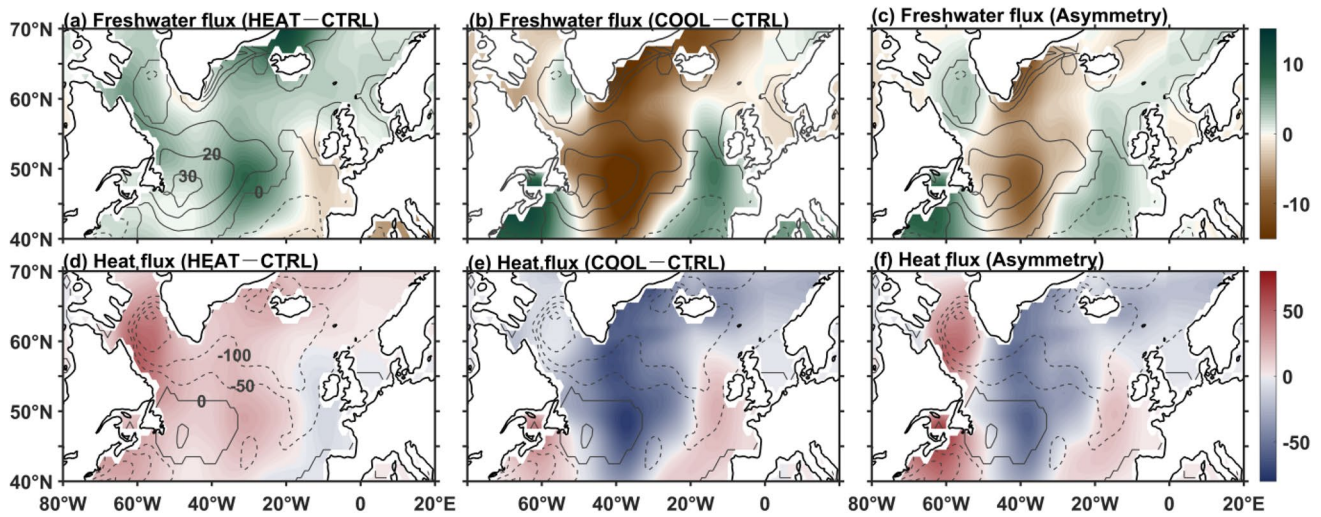

Fig. 7 Changes in freshwater flux (shading; 10^{-6} kg m^{-2} s^{-1}) and heat flux (shading; W m^{-2}) in response to the warming (**a**, **d**), the cooling (**b**, **e**), and their corresponding asymmetries (**c**, **f**), with the positive representing ocean gain heat or freshwater. The superimposed black contours are the freshwater flux and heat flux in CTRL [solid lines for ocean gain heat or freshwater and dashed lines for ocean loss heat or freshwater; contour interval is 10^{-5} kg m^{-2} s^{-1} in (**a**–**c**) and 50 W m^{-2} in (**d**–**f**)]

NADW formation, and thus leads to a strengthening and deepening of the AMOC (Fig. 4h). As shown in Figs. 4i, 7c, f, it is clear that the AMOC response is more sensitive to the cooling forcing.

Note that the asymmetric net surface heat flux in Fig. 7 is different from the additional forcing perturbation in our experiments. The forcing we apply is a pair of additional idealized forcing, ensuring the energy perturbations received by the ocean in the two simulations are measurable and perfectly symmetric. This applied forcing directly results in a change in SST, which in turn modifies the outgoing longwave, latent heat and sensible heat fluxes and thus the net surface heat flux. The results shown in Fig. 7 are the net surface heat flux changes, which are apparently not symmetric between the warming and cooling scenarios.

To understand the reason behind this asymmetry, the net surface heat flux changes are decomposed into the longwave radiation, shortwave radiation, latent heat flux and sensible heat flux. Figure 8a shows the results averaged over the subpolar North Atlantic region (SPNA; 50°N–70°N, 60°W–10°E). Under the warming (cooling), the SPNA is found to be characterized by a decrease (increase) of heat loss by the ocean, resulted mainly from changes in the sensible heat flux. However, the changes in the sensible heat flux are not symmetric, with the decrease due to the cooling exceeding the increase due to the warming, and thus result in an asymmetry in the net total heat flux. We further decompose the sensible heat flux following the bulk formula (Alexander and Scott 1997; Roberts et al. 2012):

$$Q_{SE} = \rho c_H c_p U \Delta T, \tag{7}$$

where c_p and c_H are the specific heat and heat flux coefficients, ρ is the density of air, ΔT is the difference between SST and surface air temperature (SAT), and U is the 10 m wind speed. Clearly, both the changes in the wind speed and air-sea temperature difference can influence the sensible heat flux. To examine their relative contributions, we decompose the changes in sensible heat flux into components associated with thermal anomalies ($\overline{U}\Delta T'$), wind speed anomalies ($U'\overline{\Delta T}$), and the covariance between them ($U'\Delta T'$). It is found that the thermal anomalies play a decisive role for the changes in the sensible heat flux as well as the asymmetry (Fig. 8b). To further examine the thermal anomalies in response to the warming and cooling, we examine the changes of the zonal mean SST and SAT over the SPNA. It is found that the difference between SST and SAT in the cooling is much larger than that in the warming (not shown),

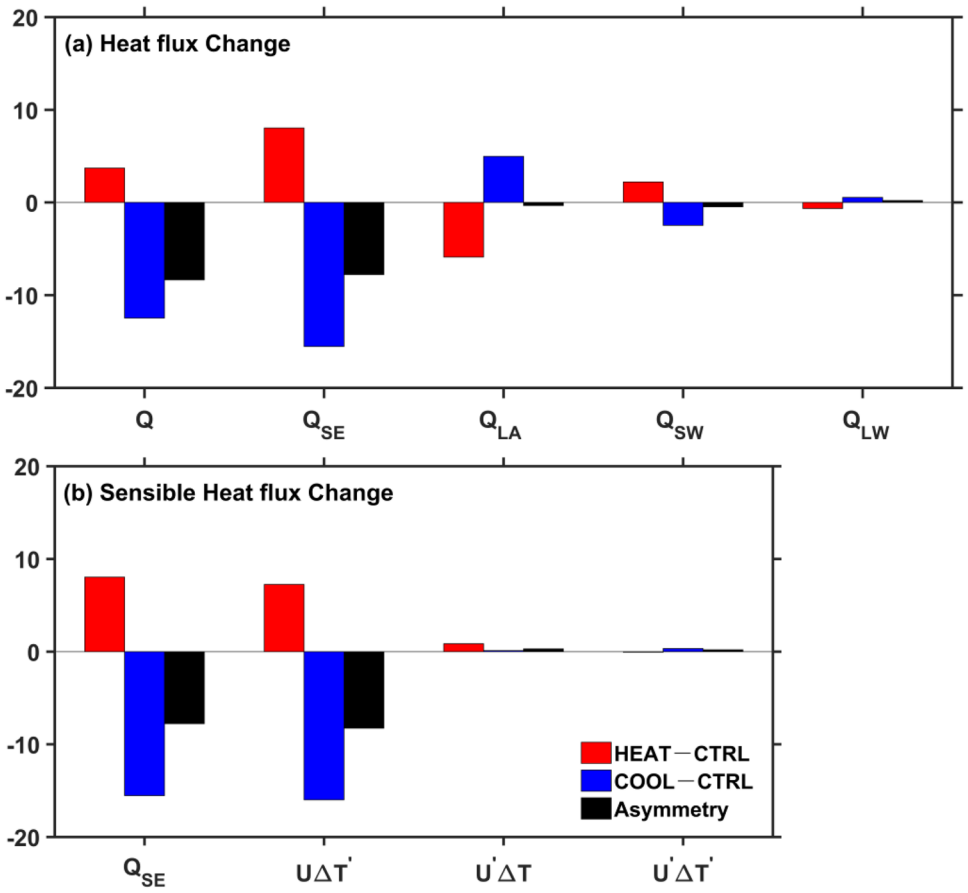

Fig. 8 Changes in **a** heat flux Q and its four components (unit: W m^{-2}) of sensible heat flux (Q_{SE}), latent heat flux (Q_{LA}), shortwave radiation (Q_{SW}) and longwave radiation (Q_{LW}), and **b** sensible heat flux and its components associated with thermal anomalies ($\overline{U}\Delta T'$), wind speed anomaly ($U'\overline{\Delta T}$), and the covariance between them ($U'\Delta T'$) averaged over the subploar North Atlantic region (50°N–70°N, 60°W–10°E). Red and blue bars stand for changes in HEAT and COOL, respectively; black bars represent their corresponding asymmetries. Note that the heat flux is averaged over ice-free regions where the sea ice concentration is less than 25% (Moore et al. 2012)

resulting in a larger change of the sensible heat flux under the cooling.

3.3 The SOMOC

Different from the Eulerian-mean dominated MOC changes in the Indo-Pacific and Atlantic basins, the total MOC changes in the Southern Ocean are maintained by a balance between the Eulerian-mean and eddy-induced components. Figure 9 shows the responses of the total SOMOC and its two components to the warming and cooling as well as their asymmetries. The Eulerian-mean SOMOC mainly represents the wind-driven Ekman circulation, which is clockwise and reaches the maximum of ~ 37 Sv at 50°S (contours in Fig. 9d). On the other hand, the eddy-induced SOMOC due to the mean buoyancy gradient (Marshall and Radko 2003) is counter-clockwise and has the maximum volume transport of ~ 11 Sv at 52ºS (contours in Fig. 9g). Therefore, the eddy-induced SOMOC partially offsets the Eulerian-mean SOMOC, and their residual is the total SOMOC with its maximum being ~ 27 Sv at 50°S (contours in Fig. 9a). These characteristics of the SOMOC are basically consistent with previous studies (Marshall and Radko 2003; Marshall et al. 2007; Viebahn and Eden 2010; Yang et al. 2015; Downes et al. 2015; Farneti et al. 2015).

In order to measure the SOMOC changes under the warming and cooling, we estimate the latitudinal position and magnitude of the core of the SOMOC (stars in Fig. 9a, b). It is found that there is a weakening (strengthening) and southward (northward) shift in the total SOMOC in response to the warming (cooling). However, their changes appear to be asymmetric, with greater change in magnitude but weaker latitudinal shift under the cooling compared to the warming.

In response to the warming, the Eulerian-mean SOMOC weakens and shifts poleward (red and black stars in Fig. 9d). On the contrary, the cooling produces a strengthening and an equatorward shift of the Eulerian-mean SOMOC (green and black stars in Fig. 9e). Their asymmetry appears to be an overall slowdown of the Eulerian-mean SOMOC (color in Fig. 9f). Since the Eulerian-mean SOMOC is wind-driven, we examine the changes of zonally averaged wind stress (Fig. 5b). It is found that the warming (cooling) induces a poleward (equatorward) shift of the wind stress and thus the Eulerian-mean SOMOC (Fig. 9d, e). Meanwhile, the

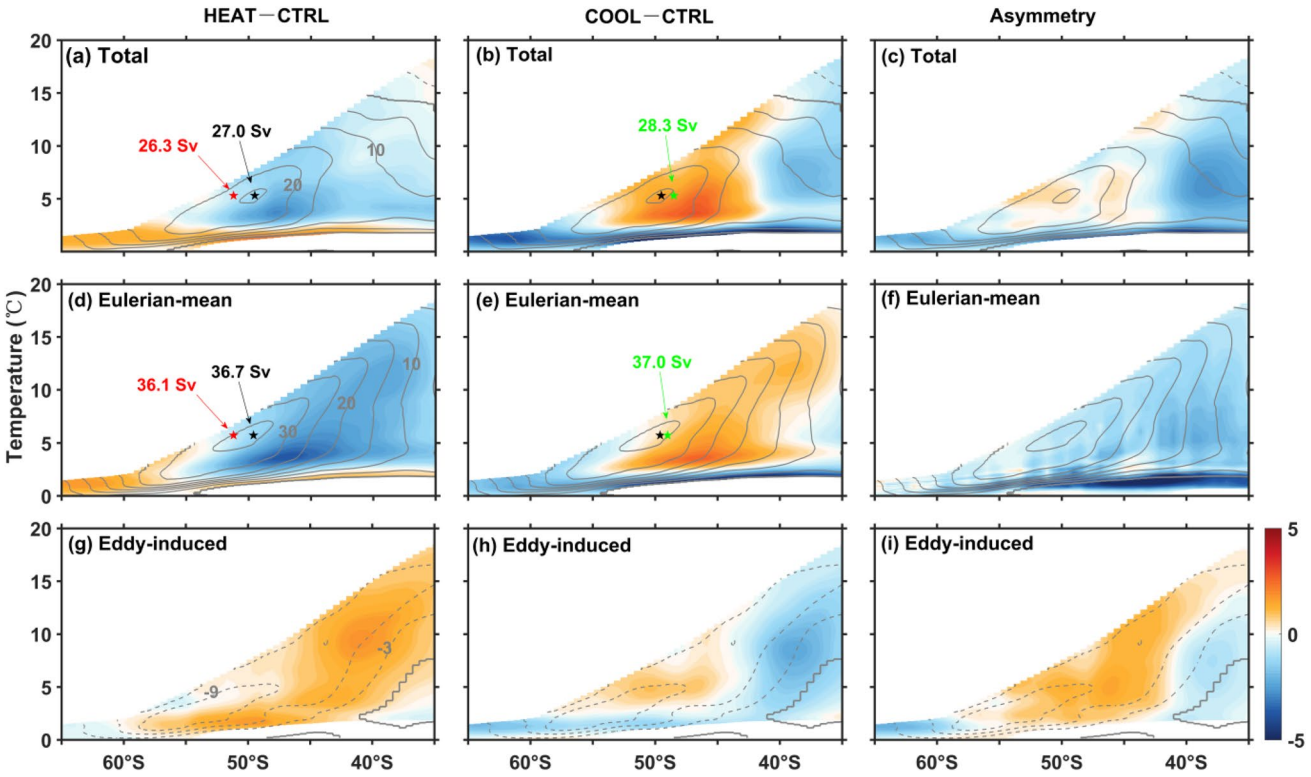

Fig. 9 Changes of the SOMOC (shading; Sv) in response to the warming (left), the cooling (middle), and their corresponding asymmetry (right). The total SOMOC (**a–c**) is the residual of the Eulerian-mean (**d–f**) and the eddy-induced (**g–i**) components. The superimposed black contours are the SOMOC in CTRL (solid lines for clockwise and dashed lines for anticlockwise; contour interval is 5 Sv in upper and middle panels and 3 Sv in lower panels). The stars in (**a**) –(**d**) represent magnitude and location of the SOMOC core, being taken as the maximum value and latitudinal position of mass transport streamfunction; black, red, and green stars stand for the SOMOC cores in CTRL, HEAT, and COOL, respectively

asymmetric change of the Eulerian-mean SOMOC (Fig. 9f) is resulted from negative anomalies in the asymmetry of the zonal wind stress over the Southern Ocean (green line in Fig. 5b).

Under the warming, the slowdown of the Eulerian-mean SOMOC (Fig. 9d) is compensated partially by the decrease of the eddy-induced SOMOC (Fig. 9g). This compensation relationship is consistent with the 'eddy compensation' theory (Viebahn and Eden 2010; Downes and Hogg 2013; Gent 2016; Poulsen et al. 2018). Under the cooling, however, the changes of the Eulerian-mean SOMOC and eddy-induced SOMOC have the same sign between 45°S to 50°S (Fig. 9e, h), and they work together to enhance the northward transport. The strength of the eddy-induced SOMOC is closely related to the tilt of isopycnals, and steeper isopycnals produce more eddies through baroclinic instability and thus have a stronger eddy-induced transport. Figure 10 shows the distribution of isopycnals in the Southern Ocean and their changes in response to the warming and cooling. It is clear that the warming induces steeper (flatter) isopycnals south (north) of 52°S, which is consistent with the wind stress change (Fig. 5b). Under the cooling, however, the isopycnals become flatter (steeper) south (north) of 45°S, which cannot be explained by the weakened (intensified) wind stress south (north) of 50°S and is likely resulted from the weakened stratification. Therefore, the 'eddy compensation' theory does not seem to work over 45°–50°S under the cooling.

4 Response of the OHT

4.1 Response patterns

Under the warming, the poleward OHT is decreased in both hemispheres (Fig. 11a). The decrease in the southern hemisphere mainly occurs over the Southern Ocean and the Indo-Pacific Ocean (Fig. 11a, d), while the decrease in the northern hemisphere is mainly confined in the Atlantic Ocean (Fig. 11g). Moreover, it is worth noting that there is an increase in OHT in the Arctic (north of 60°N) after warming (Fig. 11g). These results are consistent with the finding of Yang and Saenko (2012). The response of the OHT to the cooling (Fig. 11b) is overall a mirror image of that to the warming but with a stronger amplitude in the southern hemisphere (Fig. 11c). A decomposition finds that the changes in the total OHT are primarily determined by their Eulerian-mean components in both warming and cooling scenarios and thus their asymmetry (comparing black lines

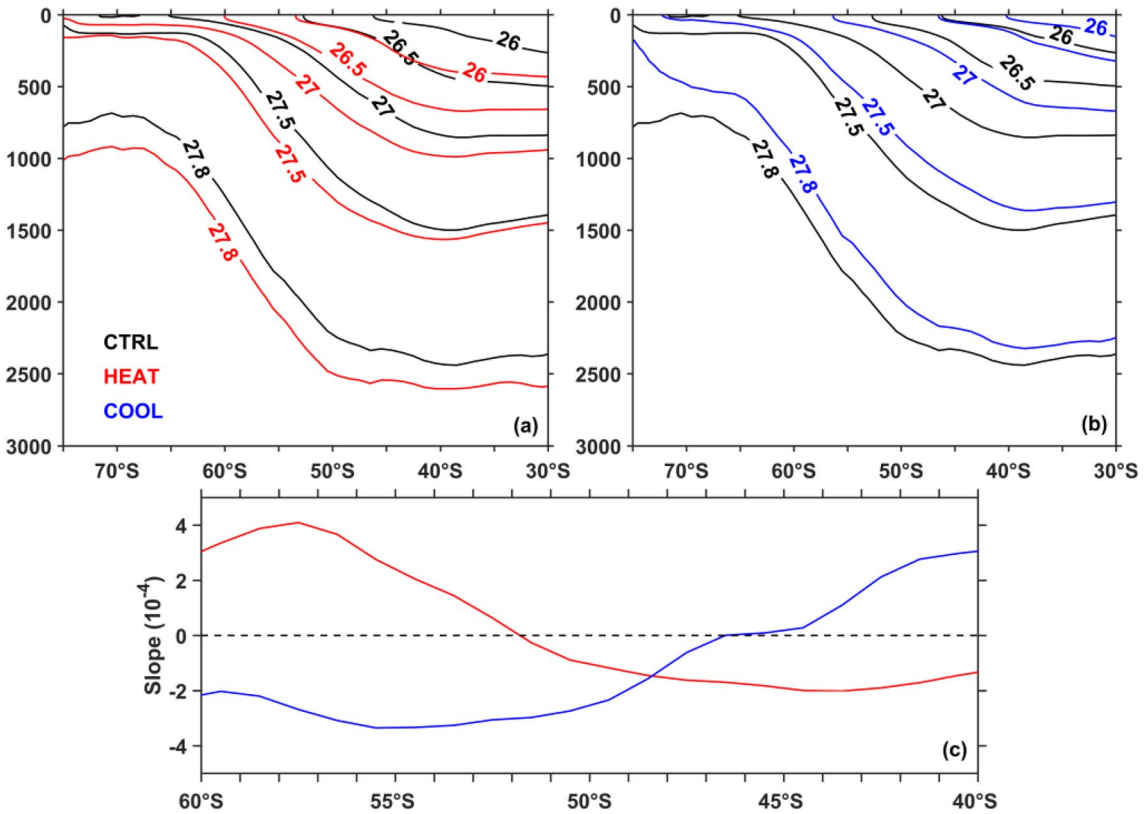

Fig. 10 Distribution of isopycnals in **a** the warming and **b** the cooling, and **c** changes of isopycnal slope averaged over 27.0–27.5 kg m^{-3} in response to the warming (red lines) and cooling (blue lines) in the Southern Ocean

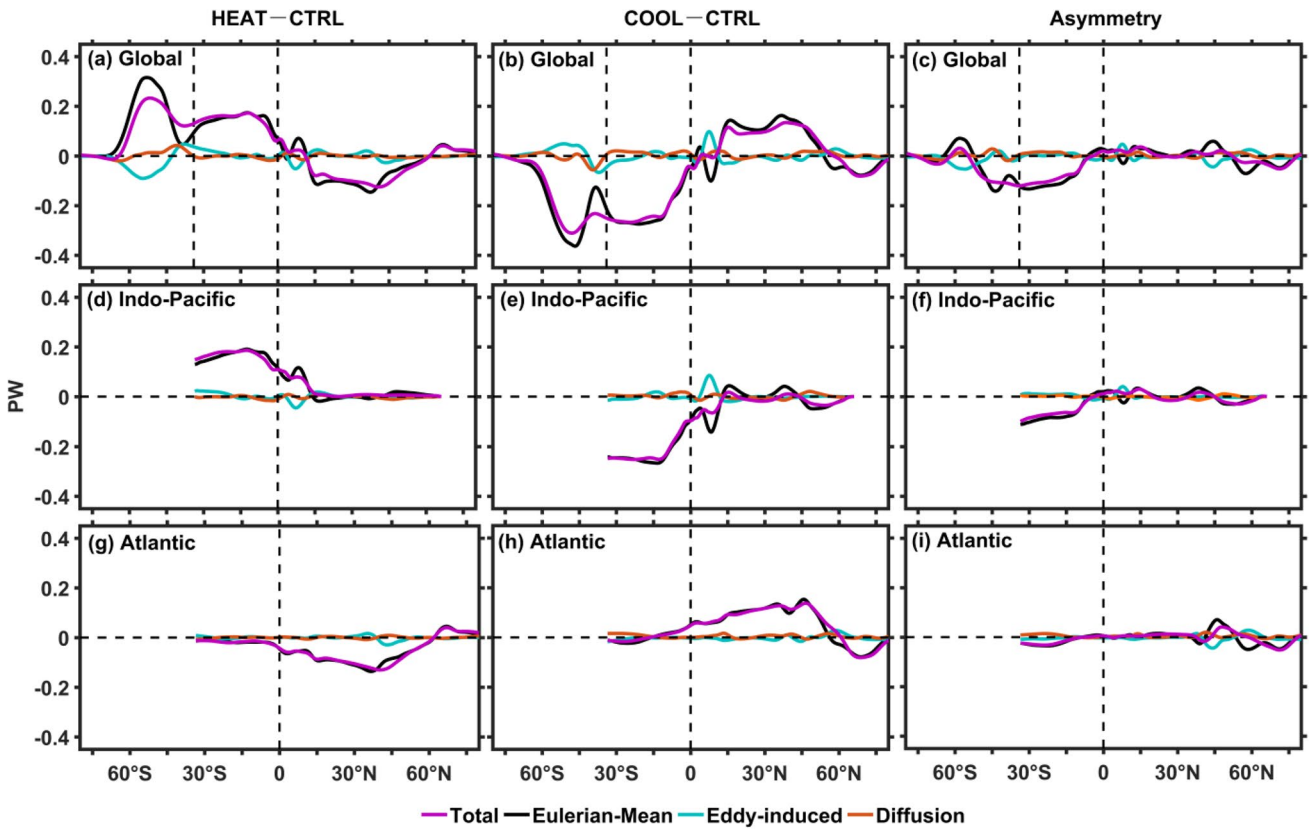

Fig. 11 The OHT changes for the Global Ocean, the Indo-Pacific Ocean, and the Atlantic Ocean in response to the warming (left), the cooling (middle) and their corresponding asymmetry (right). The total OHT (purple) is decomposed into components induced by Eulerian-mean flow (black), eddies (light blue) and diffusion (orange)

with purple lines in Fig. 11), and the contributions from the eddies and diffusion are insignificant except for the Southern Ocean. A further decomposition of the Eulerian-mean OHT into contributions from the meridional overturning cells and the horizontal gyres shows that the cell component plays a dominant role in both Indo-Pacific and Atlantic Oceans (Fig. 12d–e, g, h), indicating the importance of the STC and AMOC. However, the gyre component determines the OHT response into the Arctic (Fig. 12g–i), indicating the importance of horizontal circulation in connecting the midlatitudes and the Arctic. Besides, the gyre component also contributes largely to the asymmetry in the Southern Ocean (Fig. 12c).

In order to determine the contributions from overturning circulation and temperature changes to the OHT change, we further decompose the cell-induced Eulerian-mean OHT into the dynamic, thermodynamic, and nonlinear components (Fig. 13). North of 35°S, the cell-induced Eulerian-mean OHT is dominated by its dynamic component. Specifically, in the southern Indo-Pacific Ocean (Fig 13d, e), while the contribution of nonlinear component is negligible, the northward (southward) dynamic component overwhelms the southward (northward) thermodynamic component in response to the warming (cooling), resulting in a net northward (southward) anomaly of the cell-induced Eulerian-mean OHT. However, the cooling effect exceeds the warming effect, leading to a southward anomaly in their asymmetry there (Fig. 13f). In the Atlantic Ocean, the dynamic and thermodynamic components still act to compensate each other, and the nonlinear component appears to be southward in both scenarios (Fig. 13g, h). For their asymmetry, the accumulated southward nonlinear portion is cancelled out by the dynamic and thermodynamic portions, leading to a near-zero cell-induced Eulerian-mean OHT there (Fig. 13i). Over the Southern Ocean (south of 35°S), in stark contrast, the responses of the cell-induced Eulerian-mean OHT to both the warming and cooling, as well as their asymmetry, are all dominated by its thermodynamic component (Fig. 13a–c).

4.2 Response mechanisms

The main purpose of these above decompositions is to identify the physical mechanisms that drive the OHT changes under the warming and cooling as well as their asymmetry. In this subsection we intend to explain the formation

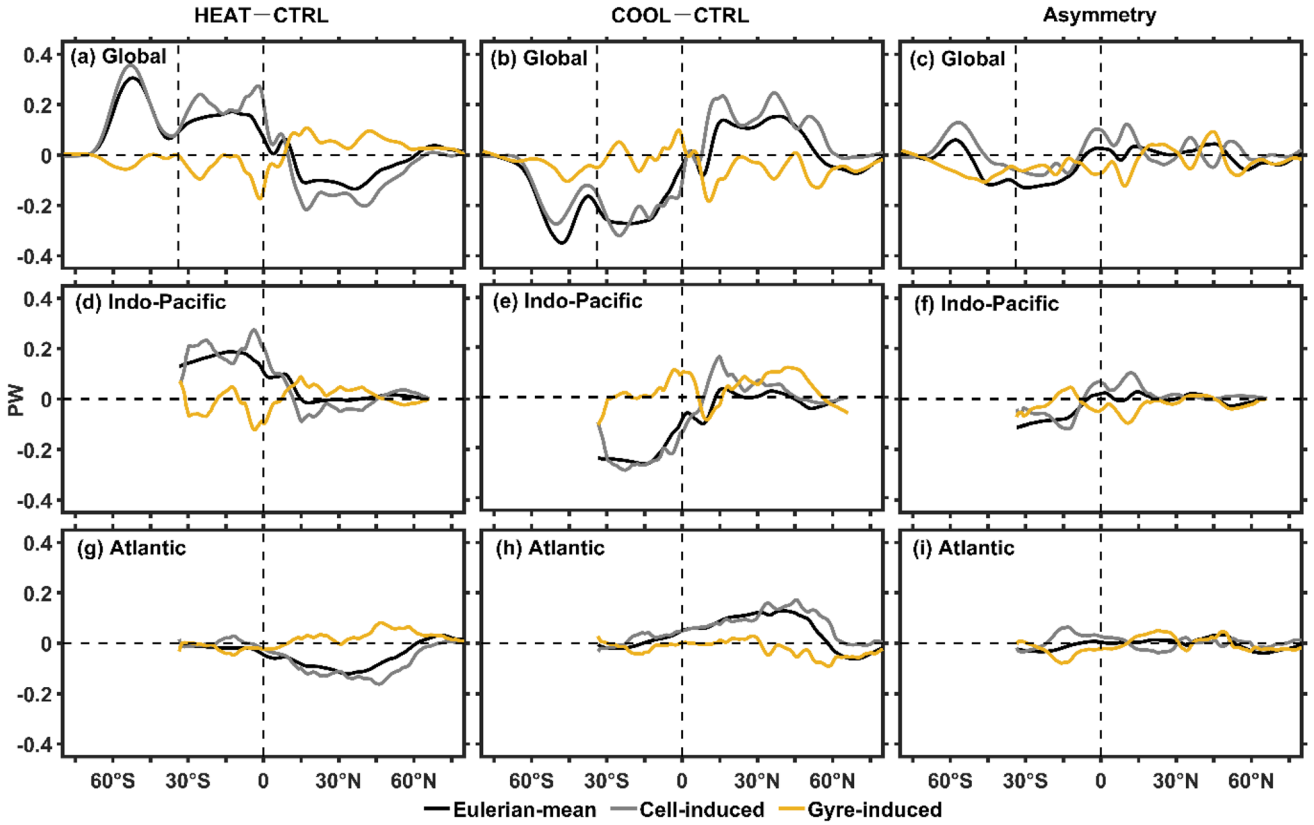

Fig. 12 Changes of the OHT_{Eul} (black) as well as its components OHT_{Cell} (grey) and OHT_{Gyre} (yellow) for the Global Ocean, the Indo-Pacific Ocean and the Atlantic Ocean in response to the warming (left), the cooling (middle) and their corresponding asymmetry (right)

processes of the OHT response patterns, which are summarized in Fig. 14 for the warming scenario over the three Oceans.

For the Indo-Pacific Ocean, major OHT responses appear in the southern hemisphere (Fig. 11d–f). Under the warming, the weakened easterlies in the southern subtropics between 10 and 30°S (Fig. 5a) slows the STC down (Fig. 4d), leading to an equatorward anomalous dynamic transport (blue line in Fig. 13d). Meanwhile, the stronger warming at ocean surface relative to the deeper ocean increases the vertical stratification (Fig. 15a), leading to a poleward anomalous thermodynamic transport (red line in Fig. 13d). Taken together, the dynamic-induced equatorward anomaly surpasses the thermodynamic-induced anomaly, resulting in a decrease of the poleward OHT (purple line in Fig. 11d). The physical processes that govern the OHT changes under the cooling are similar to those under the warming, but with an opposite sign.

For the Atlantic Ocean, the warming increases heat gain (Fig. 7d) and enhances freshwater input (Fig. 7a) over the subpolar region, leading to a more buoyant surface ocean and a deceleration of the AMOC (Fig. 4g) and thus a southward anomaly of the cell-induced Eulerian-mean OHT (blue line in Fig. 13g). Meantime, the more stratified upper ocean in response to the warming (Fig. 15d), together with the clockwise mean AMOC, lead to a northward anomaly of the cell-induced Eulerian-mean OHT (red line in Fig. 13g). The dynamic anomaly overwhelms the thermodynamic anomaly, eventually decreasing the northward mean OHT. The underlying processes operating the OHT changes under the cooling are similar to those under the warming, but with an opposite sign.

For the Southern Ocean (south of 35°S), unlike in the Indo-Pacific and Atlantic Oceans where the dynamic processes dominate the changes in the OHT, the thermodynamic processes play a decisive role for the responses. Under the warming, the stronger warming at the ocean surface relative to the deeper ocean increases the vertical stratification (Fig. 15g), leading to a large northward anomaly of the cell-induced Eulerian-mean OHT by the mean SOMOC (red line in Fig. 13a). In contrast to what happens in the Indo-Pacific and Atlantic Oceans, the northward thermodynamic anomaly overwhelms the dynamic anomaly, resulting in a northward anomalous cell-induced Eulerian-mean OHT (grey line in Fig. 13a). The latter in turn determines a northward anomaly of the Eulerian-mean OHT (black line in Fig. 12a), which is partially offset by the southward anomaly of the eddy-induced

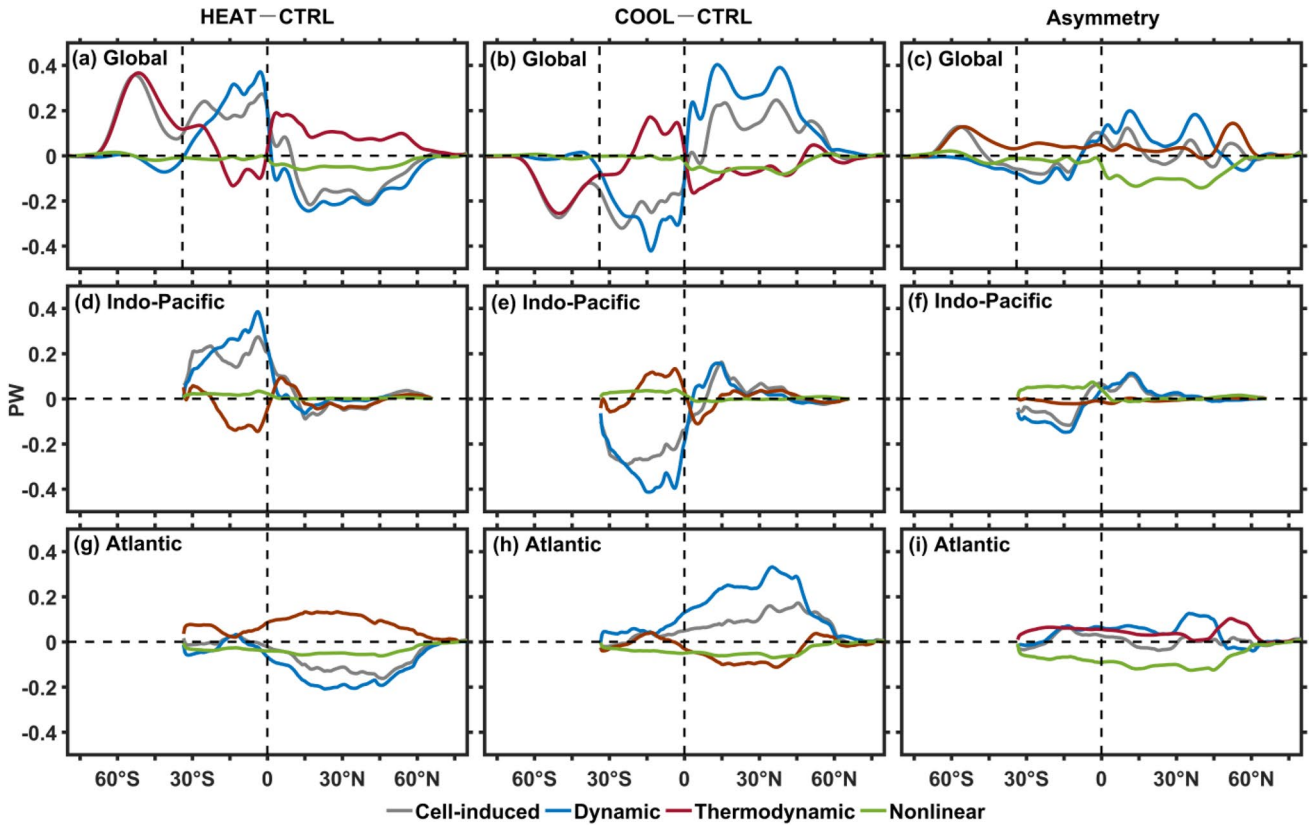

Fig. 13 Changes of the OHT_{Cell} for the Global Ocean, the Indo-Pacific Ocean and the Atlantic Ocean in response to the warming (left), the cooling (middle) and their corresponding asymmetry (right). The OHT_{Cell} (grey) is decomposed into the dynamic (blue), thermodynamic (red) and nonlinear (green) components

OHT (light blue line in Fig. 11a) and eventually leads to a northward OHT anomaly (purple line in Fig. 11a). The working processes under the cooling are similar to those under the warming, but with an opposite sign.

Regarding the asymmetric response, the response of the OHT thermodynamic component under the warming surpasses that under the cooling, resulting from the vertical structure of temperature anomaly. Specifically, owing to the inherent nonlinearity of convection (Yang and Zhu 2012; Xie et al. 2013; Manabe et al. 1991), cooling-induced convection is able to penetrate deeper than heating-induced convection, leaving a positive (negative) temperature asymmetry in the upper (deeper) ocean (colors in Fig. 15c, f, i). For this reason, the asymmetry of temperature anomaly has a similar vertical structure with the temperature anomaly under the warming, and the distribution of the thermodynamic-induced OHT asymmetry resembles that in the warming case. In contrast, the changes in dynamic component are greater under the cooling since both the AMOC and STC are more sensitive to negative heat flux anomaly (Fig. 4f, i), and thus the distribution of the dynamic-induced OHT asymmetry follows that in the cooling case. Overall, the OHT response to the warming is stronger (weaker) than that to the cooling over the regions where the thermodynamic (dynamic) processes dominate.

For the Indo-Pacific Ocean, the cooling effect surpasses the warming effect since dynamic processes dominates the OHT (purple line in Fig. 11f). For the Atlantic Ocean, while the dynamic processes still play a dominant role, the OHT responses to the warming and cooling forcings are overall symmetric due to the delicate balance among the nonlinear, dynamic and thermodynamic components (Fig. 13i). For the Southern Ocean, the response of the cell-induced OHT, which is determined by thermodynamic processes, is stronger under the warming (Fig. 13c). But the asymmetry in the cell-induced OHT response is largely compensated by the gyre-induced OHT (Fig. 12c), because the horizontal circulation changes (mainly in the ACC) in both scenarios induce a southward OHT anomaly (yellow lines in Fig. 12a, b). In addition, the eddy-induced OHT asymmetry (light blue line in Fig. 11c) resembles that in the warming scenario (light blue line Fig. 11a), likely due to the similar vertical structure of temperature anomaly between the asymmetry (color in Fig. 15i) and the warming (color in Fig. 15g). The anomalous cell-induced OHT collaborates with the gyre- and eddy-induced OHT anomalies (Fig. 11c)

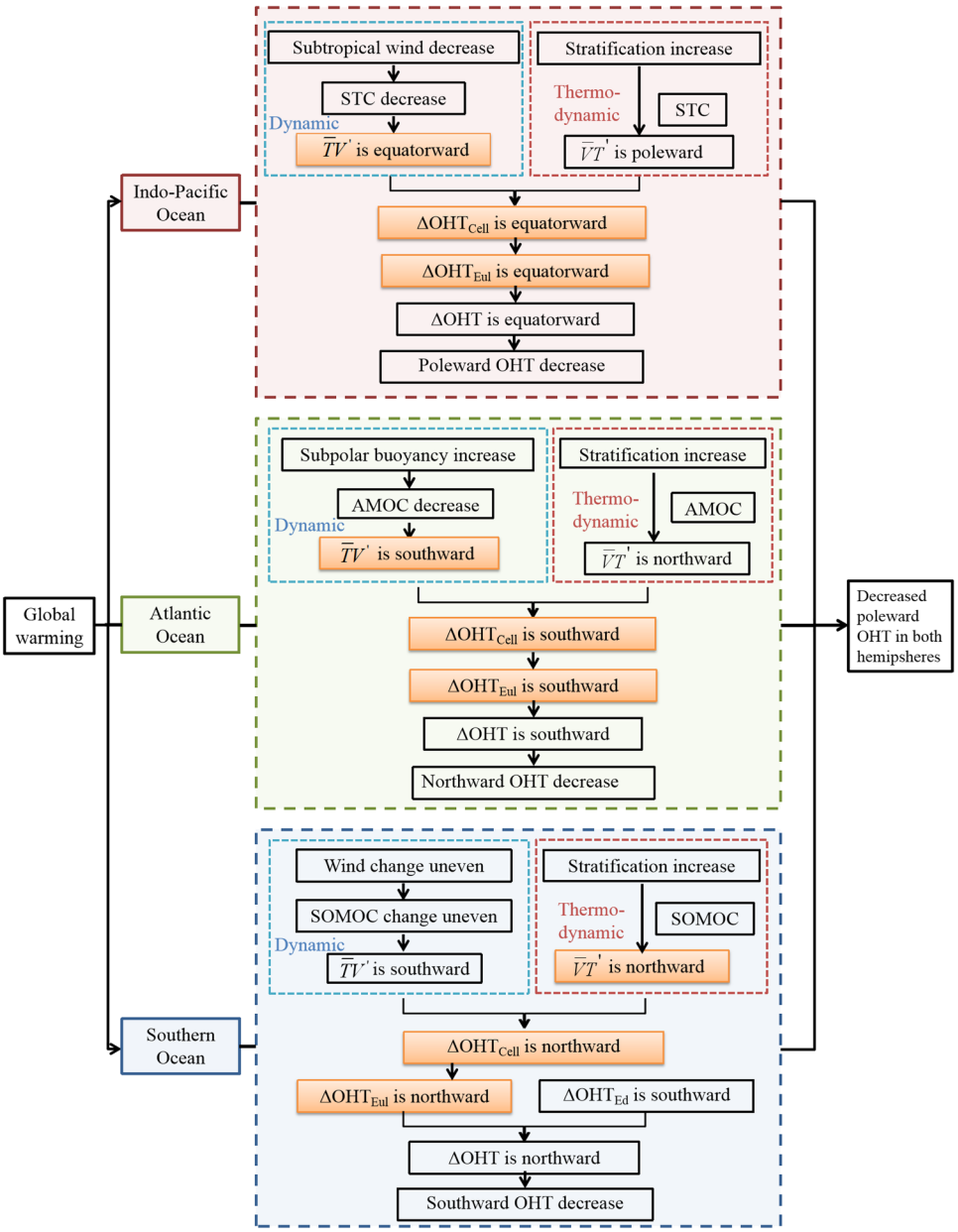

Fig. 14 A schematic diagram summarizing the underlying processes responsible for the OHT changes in response to the warming over the Indo-Pacific Ocean, the Atlantic Ocean, and the Southern Ocean. The boxes in orange highlight the dominant processes for the OHT changes

to generate a southward OHT asymmetry over the Southern Ocean except for the region between 55° and 60°S (purple line in Fig. 11c).

5 Summary and discussions

In this study, we employ the CESM to investigate the responses of the OHT to climate warming and cooling by imposing heat fluxes of equal amplitude but opposite sign into the ocean surface. The focus of this study is to examine whether the OHT responses are symmetric and understand the underlying mechanisms. The main conclusions are as follows:

- The warming (cooling) induces a weakening (strengthening) of the poleward OHT, with the cooling effect exceeding the warming effect in the southern hemisphere.
- For the Indo-Pacific and Atlantic Oceans (north of 35°S), the total responses to both the warming and cooling as well as their corresponding asymmetry are dominated by the Eulerian-mean OHT, which is further resulted from the advection of mean temperature by anomalous MOC ($\overline{TV}'$). Since the STC (AMOC) is more sensitive to the cooling than warming, the changes in the dynamic component of the OHT are greater in the former. This ultimately explains the overwhelming effect of the cooling on the OHT over the Indo-Pacific Ocean. However, in the Atlantic Ocean, the nonlinear effect of temperature

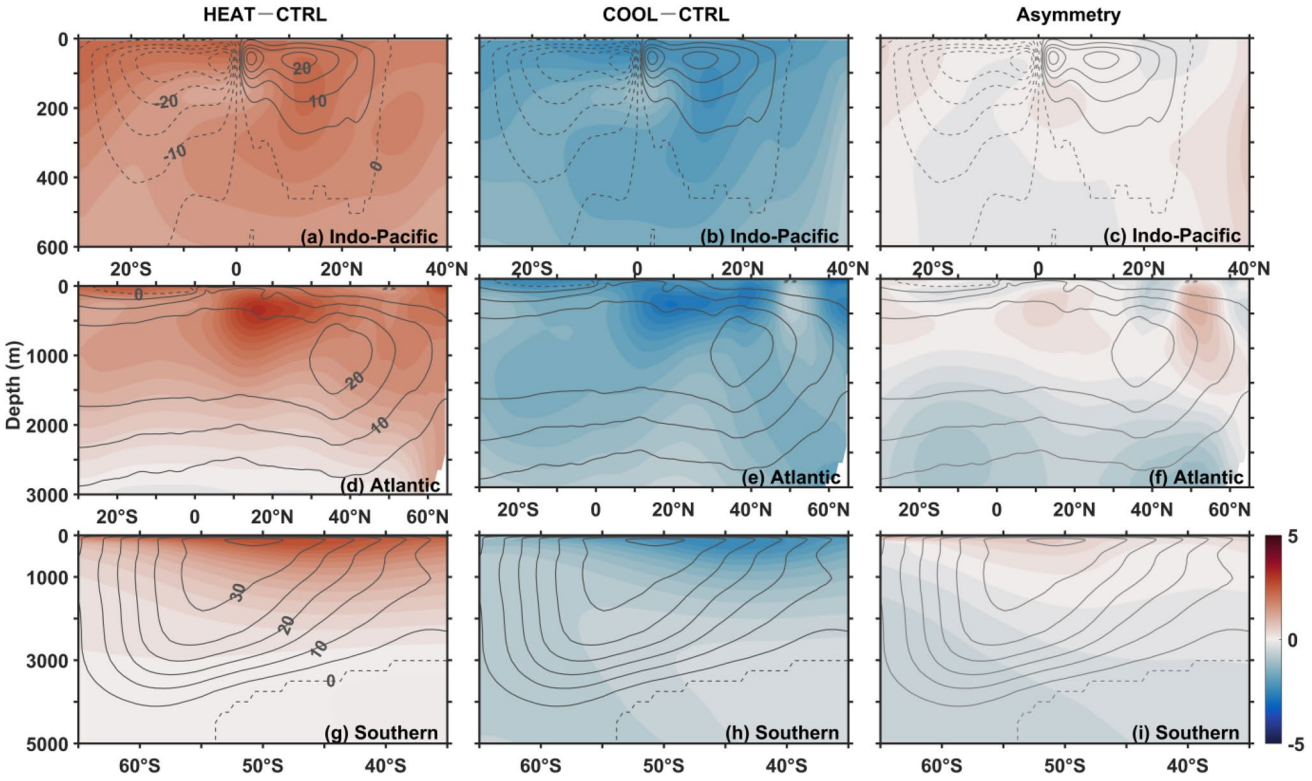

Fig. 15 Changes of zonal mean temperature (shading; °C) over the Indo-Pacific Ocean, the Atlantic Ocean, and the Southern Ocean in response to the warming (left), the cooling (middle) and their corresponding asymmetry (right). The superimposed black contours are the MOC in CTRL (solid lines for clockwise and dashed lines for anticlockwise; contour interval is 5 Sv)

and velocity changes ($T'V'$) also contributes to the asymmetric OHT response, which fully counteracts the asymmetric changes due to the dynamic and thermodynamic components and leads to a near-zero asymmetric OHT response.

- For the Southern Ocean (south of 35°S), although the total responses of the OHT to both the warming and cooling are also dominated by its Eulerian-mean component, the eddy-induced component appears to have a significant contribution and acts to compensate partially for the Eulerian-mean component. In addition, different from the situation in the Indo-Pacific and Atlantic Oceans, the Eulerian-mean component in the Southern Ocean is primarily resulted from the advection of anomalous temperature by mean clockwise SOMOC ($\overline{V}T'$), while the SOMOC change ($\overline{T}V'$) has less contribution. Moreover, the asymmetric OHT response is a joint effort among the overturning circulation cells, horizontal gyres, eddies, as well as temperature changes in the Southern Ocean.

The response of the OHT to the positive heat flux in our simulation is in accordance with that to anthropogenic warming in climate models (e.g., Yang and Saenko 2012; Liu et al., 2018; He et al. 2019; Donohoe et al. 2020). While being in agreement with a majority of these existing studies on the warming-induced OHT changes over the Indo-Pacific and Atlantic Oceans, our findings support the study of He et al. (2019) who found that, compared with the overturning circulation changes, the vertical temperature structure changes have larger impacts on the OHT changes over the Southern Ocean. In addition, we find that the horizontal circulation changes also contribute to the OHT response in the Southern Ocean, especially for its asymmetry. Moreover, the change of the horizontal circulation in the Southern Ocean is found to enhance the southward OHT in both the warming and cooling scenarios, which further points to the uniqueness of this region.

Existing modelling studies have shown that there exists a compensated change of OHT and AHT during their initial responses to global warming, with a decreasing poleward OHT and an increasing poleward AHT in both hemispheres (Held and Soden 2006; Vellinga and Wu 2008; Zelinka and Hartmann 2012; Rose and Ferreira 2013; Yang and Dai 2015; Yang et al. 2018; Harrop et al. 2018). Figure 16 shows the OHT, AHT and total meridional heat transport as well as their changes in response to the warming with CESM. Regarding the response to the warming (Fig. 16b), as discussed above, we find a decrease of the

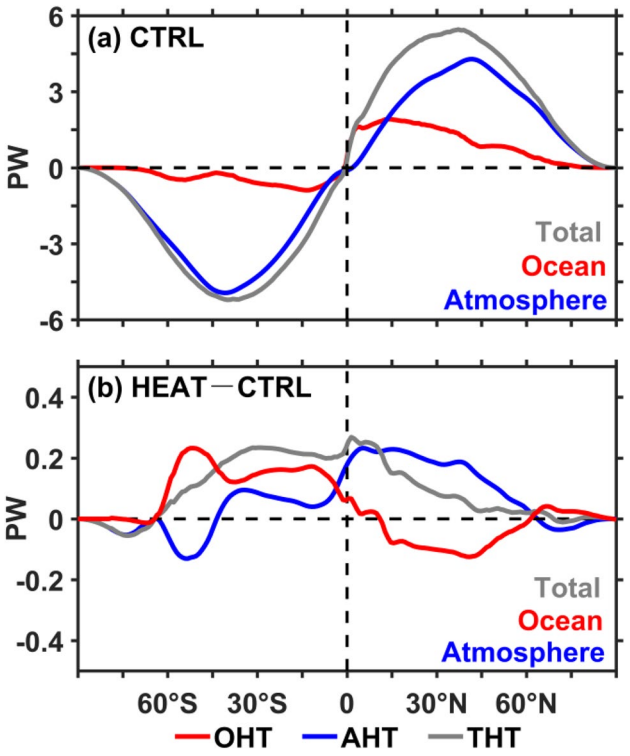

Fig. 16 The OHT, meridional atmosphere heat transport (AHT), and total meridional heat transport (THT) in **a** CTRL and **b** their changes in response to the warming (positive for northward transport)

poleward OHT in both hemispheres, which is also consistent with previous modelling. However, it is surprising to see that the AHT and OHT changes in the low- to mid-latitudes of the southern hemisphere are of the same direction, and work together to transfer energy northward in our warming simulation (Fig. 16b). Apart from this region, the change in the OHT is overall compensated by the change in the AHT. This might arise from the warming setting in our simulation. To be specific, the HEAT simulation in this study is carried out through adding a uniform heat flux into the ocean surface and integrated for 250 years. By this way, both the upper ocean and the atmosphere are able to reach a quasi-equilibrium stage after 150 years of model integration, although the deep ocean is still adjusting. We speculate that if our HEAT experiment is further integrated for a few more centuries, the relationship of AHT and OHT would be similar to what He et al. (2019) found during the later stage of global warming in their simulations.

We would like to point out that the CESM does not resolve mesoscale eddies in the ocean, which may cause doubt about its ability to simulate the eddy-induced OHT and its changes under different forcings, especially in the Southern Ocean where eddies can account for a large portion of the total energy transport. Therefore, further studies with high-resolution eddy-resolving model are needed to address this issue.

Acknowledgements We thank three anonymous reviewers for their valuable comments that helped improve the manuscript. This work is supported by the National Key Research and Development Program of China (2018YFA0605702) and the National Natural Science Foundation of China (NSFC; 41906002, 41976006, 41676002 and 91858210). The CMIP6 simulations are available via the Earth System Grid Federation (ESGF) archive (https://esgf-node.llnl.gov/projects/esgf-llnl/).

Author contributions YL and FL were responsible for design of the research. QL analyzed the data and wrote the first draft of the manuscript and YL and FL helped with the revision of the manuscript. All authors read and approved the revised manuscript.

Funding This work was supported by the National Key Research and Development Program of China (2018YFA0605702) and the National Natural Science Foundation of China (NSFC; 41906002, 41976006, 41676002 and 91858210).

Availability of data and material The datasets used in this study are available from the corresponding authors upon request. The CMIP6 data are publicly available through the Earth System Grid Federation (ESGF) archive (https://esgf-node.llnl.gov/projects/esgf-llnl/).

Code availability Scripts for analysing the data are available from the corresponding authors upon request.

Declarations

Conflict of interest The authors declare no competing interests.

Ethics approval Not applicable.

Consent to participate Not applicable.

Consent for publication Not applicable.

References

Adam O, Bischoff T, Schneider T (2016) Seasonal and interannual variations of the energy flux equator and ITCZ. Part I: zonally averaged ITCZ position. J Clim 29:3219–3230

Alexander MA, Scott JD (1997) Surface flux variability over the North Pacific and North Atlantic Oceans. J Clim 10:2963–2978

Bakker P, Schmittner A, Lenaerts JTM, Abe-Ouchi A, Bi D, van den Broeke MR, Chan W-L, Hu A, Beadling RL, Marsland SJ, Mernild SH, Saenko OA, Swingedouw D, Sullivan A, Yin J (2016) Fate of the Atlantic Meridional Overturning Circulation: strong decline under continued warming and Greenland melting. Geophys Res Lett 43:12252–12260

Boccaletti G, Ferrari R, Adcroft A, Ferreira D, Marshall J (2005) The vertical structure of ocean heat transport. Geophys Res Lett 32:L10603. https://doi.org/10.1029/2005GL022474

Bryan K (1962) Measurements of meridional heat transport by ocean currents. J Geophys Res 67:3403–3414

Bryan K (1982) Poleward heat transport by the ocean: observations and models. Ann Rev Earth Planet Sci 10:15–38

Cheng W, Chiang JCH, Zhang D (2013) Atlantic Meridional Overturning Circulation (AMOC) in CMIP5 models: RCP and historical simulations. J Clim 26:7187–7197

Deng J, Dai A, Xu H (2020) Nonlinear climate responses to increasing CO_2 and anthropogenic aerosols simulated by CESM1. J Clim 33:281–301

Donohoe A, Armour KC, Roe GH, Battisti DS, Hahn L (2020) The partitioning of meridional heat transport from the last glacial maximum to CO_2 quadrupling in coupled climate models. J Clim 33:4141–4165

Downes SM, Hogg AM (2013) Southern ocean circulation and eddy compensation in CMIP5 models. J Clim 26:7198–7220

Downes SM, Farneti R, Uotila P, Griffies SM, Marsland SJ, Bailey D et al (2015) An assessment of Southern Ocean water masses and sea ice during 1988–2007 in a suite of interannual CORE-II simulations. Ocean Model 94:67–94

Farneti R, Dwivedi S, Kucharski F, Molteni F, Griffies SM (2014) On pacific subtropical cell variability over the second half of the twentieth century. J Clim 27:7102–7112

Farneti R, Downes SM, Griffies SM, Marsland SJ, Behrens E, Bentsen M et al (2015) An assessment of antarctic circumpolar current and southern ocean meridional overturning circulation during 1958–2007 in a suite of interannual core-ii simulations. Ocean Model 93:84–120

Ferrari R, Ferreira D (2011) What processes drive the ocean heat transport? Ocean Model 38:171–186

Fox-Kemper B, Ferrari R, Hallberg R (2008) Parameterization of mixed layer Eddies. Part I: theory and diagnosis. J Phys Oceanogr 38:1145–1165

Ganachaud A, Wunsch C (2000) Improved estimates of global ocean circulation, heat transport and mixing from hydrographic data. Nature 408:453–457

Ganachaud A, Wunsch C (2003) Large-scale ocean heat and freshwater transports during the World Ocean Circulation Experiment. J Clim 16:696–705

Gent PR (2016) Effects of southern hemisphere wind changes on the meridional overturning circulation in ocean models. Ann Rev Mar Sci 8:79–94

Gent PR, McWilliams JC (1990) Isopycnal mixing in ocean circulation models. J Phys Oceanogr 20:150–155

Green B, Marshall J (2017) Coupling of trade winds with ocean circulation damps ITCZ shifts. J Clim 30:4395–4411

Gregory JM (2004) A new method for diagnosing radiative forcing and climate sensitivity. Geophys Res Lett 31:L03205. https://doi.org/10.1029/2003GL018747

Gregory JM, Dixon KW, Stouffer RJ, Weaver AJ, Driesschaert E, Eby M, Fichefet T, Hasumi H, Hu A, Jungclaus JH, Kamenkovich IV, Levermann A, Montoya M, Murakami S, Nawrath S, Oka A, Sokolov AP, Thorpe RB (2005) A model intercomparison of changes in the Atlantic thermohaline circulation in response to increasing atmospheric CO_2 concentration. Geophys Res Lett 32:L12703. https://doi.org/10.1029/2005GL023209

Hall MM, Bryden HL (1982) Direct estimates and mechanisms of ocean heat transport. Deep Sea Res Part A Oceanogr Res Pap 29:339–359

Harrop BE, Lu J, Liu F, Garuba OA, Leung LR (2018) Sensitivity of the ITCZ location to ocean forcing via Q-Flux Green's function experiments. Geophys Res Lett 45:13116–13123. https://doi.org/10.1029/2018GL080772

He C, Liu Z, Hu A (2019) The transient response of atmospheric and oceanic heat transports to anthropogenic warming. Nat Clim Change 9:222–226

Held IM (2001) The partitioning of the poleward energy transport between the tropical ocean and atmosphere. J Atmos Sci 58:943–948

Held IM, Soden BJ (2006) Robust responses of the hydrological cycle to global warming. J Clim 19:5686–5699. https://doi.org/10.1175/JCLI3990.1

Hsiung J (1985) Estimates of global oceanic meridional heat transport. J Phys Oceanogr 15:1405–1413

Jahn A, Holland MM (2013) Implications of Arctic sea ice changes for North Atlantic deep convection and the meridional overturning circulation in CCSM4-CMIP5 simulations. Geophys Res Lett 40:1206–1211

Kang SM, Shin Y, Xie S-P (2018) Extratropical forcing and tropical rainfall distribution: energetics framework and ocean Ekman advection. NPJ Clim Atmos Sci 1:1–10

Li Z, Luo Y (2018) Response of the tropical Indian Ocean to greenhouse gases versus aerosol forcing in the GFDL CM3 coupled climate model. Atmos Ocean 56:1–15

Liu W, Xie SP, Liu Z, Zhu J (2017a) Overlooked possibility of a collapsed Atlantic Meridional Overturning Circulation in warming climate. Sci Adv 3:e1601666. https://doi.org/10.1126/sciadv.1601666

Liu F, Luo Y, Lu J, Garuba O, Wan X (2017b) Asymmetric response of the equatorial pacific SST to climate warming and cooling. J Clim 30:7255–7270

Liu W, Lu J, Xie SP, Fedorov A (2018) Southern ocean heat uptake, redistribution and storage in a warming climate: the role of meridional overturning circulation. J Clim 31(12):4727–4743

Luo Y, Lu J, Liu F, Liu W (2015) Understanding the El Niño-like oceanic response in the tropical Pacific to global warming. Clim Dyn 45:1945–1964

Macdonald A, Wunsch MC (1996) An estimate of global ocean circulation and heat fluxes. Nature 382:436–439

Manabe S, Stouffer RJ, Spelman MJ, Bryan K (1991) Transient responses of a coupled ocean–atmosphere model to gradual changes of atmospheric CO_2. Part I: annual mean response. J Clim 4:785–818

Marshall J, Radko T (2003) Residual-mean solutions for the Antarctic Circumpolar Current and its associated overturning circulation. J Phys Oceanogr 33:2341–2354

Marshall J, Ferreira D, Campin JM, Enderton D (2007) Mean climate and variability of the atmosphere and ocean on an aquaplanet. J Atmos Sci 64:4270–4286

McCreary JP, Lu P (1994) Interaction between the subtropical and equatorial ocean circulations: the subtropical cell. J Phys Oceanogr 24:466–497

McPhaden MJ, Zhang D (2002) Slowdown of the meridional overturning circulation in the upper Pacific Ocean. Nature 415:603–608

Menary MB, Robson J, Allan RP, Booth BBB, Cassou C, Gastineau G, Gregory J, Hodson D, Jones C, Mignot J, Ringer M, Sutton R, Wilcox L, Zhang R (2020) Aerosol-forced AMOC changes in CMIP6 historical simulations. Geophys Res Lett. https://doi.org/10.1029/2020GL088166

Moore G, Renfrew IA, Pickart RS (2012) Spatial distribution of air-sea heat fluxes over the sub-polar North Atlantic Ocean. Geophys Res Lett 39:L18806. https://doi.org/10.1029/2012GL053097

Myhre G, Shindell D, Bréon F-M, Collins W, Fuglestvedt J, Huang J, Koch D, Lamarque J-F, Lee D, Mendoza B, Nakajima T, Robock A, Stephens G, Takemura T, Zhang H (2013) Anthropogenic and natural radiative forcing. In: Stocker TF, Qin D, Plattner G-K, Tignor M, Allen SK, Doschung J, Nauels A, Xia Y, Bex V, Midgley PM (eds) Climate change 2013: the physical science basis. Contribution of Working Group I to the Fifth Assessment Report of the Intergovernmental Panel on Climate Change. Cambridge University Press, pp 659–740. https://doi.org/10.1017/CBO9781107415324.018

Poulsen MB, Jochum M, Nuterman R (2018) Parameterized and resolved southern ocean eddy compensation. Ocean Model 124:1–15

Rahmstorf S (2002) Ocean circulation and climate during the past 120,000 years. Nature 419:207–214

Rahmstorf S, Box JE, Feulner G, Mann ME, Robinson A, Rutherford S et al (2015) Exceptional twentieth-century slowdown in Atlantic Ocean Overturning Circulation. Nat Clim Change 5:475–480

Roberts JB, Robertson FR, Clayson CA, Bosilovich MG (2012) Characterization of turbulent latent and sensible heat flux exchange between the atmosphere and ocean in MERRA. J Clim 25:821–838

Rose BE, Ferreira D (2013) Ocean heat transport and water vapor greenhouse in a warm equable climate: a new look at the low gradient paradox. J Clim 26:2117–2136. https://doi.org/10.1175/JCLI-D-11-00547.1

Schmittner A, Latif M, Schneider B (2005) Model projections of the North Atlantic thermohaline circulation for the 21st century assessed by observations. Geophys Res Lett 32:L23710. https://doi.org/10.1029/2005gl024368

Schneider T (2017) Feedback of atmosphere-ocean coupling on shifts of the intertropical convergence zone. Geophys Res Lett 44:11644–11653

Simmons HL, Jayne SR, Laurent LCS, Weaver AJ (2004) Tidally driven mixing in a numerical model of the ocean general circulation. Ocean Model 6:245–263

Solomon A, Zhang D (2006) Pacific subtropical cell variability in coupled climate model simulations of the late 19th–20th century. Ocean Model 15(3):236–249

Trenberth KE, Caron JM (2001) Estimates of meridional atmosphere and ocean heat transports. J Clim 14:3433–3443

Trenberth KE, Solomon A (1994) The global heat balance: heat transports in the atmosphere and ocean. Clim Dyn 10:107–134

Trenberth KE, Zhang Y, Fasullo J, Cheng L (2019) Observation-based estimates of global and basin ocean meridional heat transport time series. J Clim 32:4567–4583

Vellinga M, Wu P (2008) Relations between northward ocean and atmosphere energy transports in a coupled climate model. J Clim 21:561–575. https://doi.org/10.1175/2007JCLI1754.1

Viebahn J, Eden C (2010) Towards the impact of eddies on the response of the Southern Ocean to climate change. Ocean Model 34:150–165

Wang H, Xie SP, Liu Q (2016) Comparison of climate response to anthropogenic aerosol versus greenhouse gas forcing: distinct patterns. J Clim 29:5175–5188

Weaver AJ, Eby M, Kienast M, Saenko OA (2007) Response of the Atlantic meridional overturning circulation to increasing atmospheric CO_2: sensitivity to mean climate state. Geophys Res Lett 34:L05708. https://doi.org/10.1029/2006gl028756

Weaver AJ, Sedláček J, Eby M, Alexander K, Crespin E, Fichefet T, Philippon-Berthier G, Joos F, Kawamiya M, Matsumoto K, Steinacher M, Tachiiri K, Tokos K, Yoshimori M, Zickfeld K (2012) Stability of the Atlantic Meridional Overturning Circulation: a model intercomparison. Geophys Res Lett 39:L20709. https://doi.org/10.1029/2012gl053763

Weijer W, Cheng W, Garuba OA, Hu A, Nadiga BT (2020) CMIP6 models predict significant 21st century decline of the Atlantic meridional overturning circulation. Geophys Res Lett. https://doi.org/10.1029/2019GL086075

Wen Q, Yao J, Döös K, Yang H (2018) Decoding hosing and heating effects on global temperature and meridional circulations in a warming climate. J Clim 31:9605–9623

Xie S-P, Lu B, Xiang B (2013) Similar spatial patterns of climate responses to aerosol and greenhouse gas changes. Nat Geosci 6:828–832

Yang H (2011) Equilibrium thermal response timescale of global oceans. Geophys Res Lett 38:L14711. https://doi.org/10.1029/2011GL048076

Yang H, Dai H (2015) Effect of wind forcing on the Meridional heat transport in a coupled climate model: equilibrium response. Clim Dyn 45:1451–1470

Yang D, Saenko OA (2012) Ocean heat transport and its projected change in CanESM2. J Clim 25:8148–8163

Yang H, Li Q, Wang K, Sun Y, Sun D (2015) Decomposing the meridional heat transport in the climate system. Clim Dyn 44:2751–2768

Yang Q, Zhao Y, Wen Q, Yao J, Yang H (2018) Understanding Bjerknes Compensation in Meridional heat transports and the role of freshwater in a warming climate. J Clim 31:4791–4806

Yu S, Pritchard MS (2019) A strong role for the AMOC in partitioning global energy transport and shifting ITCZ position in response to latitudinally discrete solar forcing in the CESM1.2. J Clim 32:2207–2226

Zelinka MD, Hartmann DL (2012) Climate feedbacks and their implications for poleward energy flux changes in a warming climate. J Clim 25:608–624

Zhu J, Liu Z, Zhang J, Liu W (2015) AMOC response to global warming: dependence on the background climate and response timescale. Clim Dyn 44:3449–3468